LETTER • OPEN ACCESS

Direct measurements of counter-streaming flows in a low-shear stellarator magnetic island topology

OPEN ACCESS
IOP Publishing | International Atomic Energy Agency
Nuclear Fusion
Nucl. Fusion **59** (2019) 124003 (7pp)
https://doi.org/10.1088/1741-4326/ab4320

Letter

Direct measurements of counter-streaming flows in a low-shear stellarator magnetic island topology

V. Perseo[1], F. Effenberg[2,3], D. Gradic[1], R. König[1], O.P. Ford[1], F. Reimold[1], D.A. Ennis[4], O. Schmitz[2], T. Sunn Pedersen[1] and the W7-X Team[1]

[1] Max-Planck-Institut für Plasmaphysik, 17491 Greifswald, Germany
[2] Department of Engineering Physics, University of Wisconsin, Madison, WI 53706, United States of America
[3] Princeton Plasma Physics Laboratory, Princeton University, Princeton, NJ 08543, United States of America
[4] Auburn University, Auburn, AL 36849, United States of America

E-mail: valeria.perseo@ipp.mpg.de

Received 3 June 2019, revised 9 September 2019
Accepted for publication 10 September 2019
Published 26 September 2019

Abstract

We report on the first experimental verification of theoretically predicted multiple bundles of counter-streaming plasma flows in the island-divertor scrape-off layer (SOL) of the stellarator Wendelstein 7-X. In the standard toroidal field direction (counter-clockwise when looking from the top) experiments, the overall structure of the SOL flows, such as flow directions, the number of flow bundles and the magnitude of the flow velocities, are consistent with numerical predictions obtained with EMC3-EIRENE. However, the modelling does not predict changes of the flow patterns with reversal of the magnetic field direction, which are experimentally observed. This indicates that additional relevant physics, such as particle drifts, will need to be incorporated into the numerical model to better describe the whole stellarator scrape-off layer behaviour.

Keywords: island divertor, magnetic islands, scrape-off layer, impurity transport, plasma flows, coherence imaging spectroscopy

(Some figures may appear in colour only in the online journal)

1. Introduction

One of the major challenges magnetic confinement fusion devices must overcome is the issue of power and particle exhaust [1]. In future reactors [2–4], hundreds of MWs of power will stream out from the confined plasma region (core) and must be dissipated before reaching the plasma-facing components (PFCs). Otherwise, melting [5] and excessive erosion [6] will lead to short lifetimes of the PFCs and to release of impurities, with subsequent contamination of the confined plasma and performance degradation [7].

The most successfully investigated exhaust concept is a divertor, characterized by dedicated plasma-wall interaction zones where particles and heat stream to, moving parallel to the open magnetic field lines in the scrape-off layer (SOL). However, the fast parallel heat transport leads to very localized heat deposition on the targets. Empirically-determined scaling laws indicate that the heat flux deposition profile width, for a

reactor-size device modelled on tokamaks [8], results in local heat loads exceeding the material limits of known PFCs [9]. Nonetheless, for tokamaks, the single-null divertor configuration has proven effective in providing efficient power dissipation in the plasma (impurity seeding) and good particle pumping capabilities [10–12]. In stellarators, several different edge topologies have been proposed and used to form a divertor for particle and heat exhaust [13–18]. One such concept is the *island divertor* [19], which uses the intrinsic magnetic islands in the SOL to set up a divertor volume. This was successfully tested in the Wendelstein 7-AS (W7-AS) stellarator [20], and is now being investigated in more detail and at a larger scale in Wendelstein 7-X (W7-X) [21, 22].

A particular feature predicted for the island divertor topology is the existence of multiple, adjacent counter-streaming flow regions at the plasma edge. Strong counter-streaming flows are expected to lead to frictional dissipation of momentum, causing a reduction of the flow speed parallel to the magnetic field lines [23]. This is likely to have played a role in substantial heat flux mitigation at the targets [24]. According to the heuristic-drift model in [25], reduced parallel flow velocities in the SOL due to momentum dissipation could potentially lead to a widening of the SOL itself, contributing to prolong the lifetime of the PFCs. The involved physics in the counter-streaming flows includes turbulence, transverse viscosity and momentum transport. In particular, experimental observations often show larger momentum transport perpendicular to the magnetic field than expected from binary collisions. This additional transport, driven by *anomalous viscosity*, is also invoked in tokamaks applications, where rotation of the core, potentially driven by radially transported momentum from SOL flows [26], has profound effects on the macroscopic stability of the overall plasma, and thereby on the energy confinement [27]. Thus, the ability to measure detailed two-dimensional flow-maps, such as the ones presented, should help improve our understanding of such phenomena. The importance of 2D measurements for better stellarator physics insights have been already demonstrated on the Large Helical Device (LHD) as well [28, 29].

The counter-streaming structures discussed above have been predicted for multiple different stellarators, such as LHD [30, 31], W7-AS [32] and W7-X [23, 33, 34]. Compared to LHD [35], the flow pattern is expected to play a major role for a low-shear machine like W7-X [17]. Here, it has been experimentally confirmed with a view on the complete machine edge for the first time. The measurements were made with a coherence imaging spectroscopy (CIS) diagnostic, which is an interferometer able to measure 2D patterns of line-of-sight-integrated Doppler velocities of particles in the plasma [36]. The CIS measurements are compared with EMC3-EIRENE simulations, a code capable of modelling the behavior of plasmas in 3D magnetic fields [37, 38] that already showed good results for recent stellarator experiments [23, 33, 39–45]. CIS measurements for experiments with the same magnetic topology but with the field direction reversed are presented. The preliminary results of the field reversal experiments clearly demonstrate that transport physics processes in the edge are complex and not entirely described by the simplified model in the next section or the numerical tool EMC3-EIRENE.

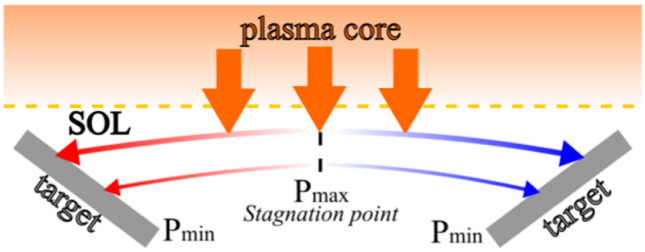

Figure 1. Sketch of a 1D SOL model. The red/blue arrows indicate the toroidal direction, along/opposite to the magnetic field.

2. Predictions

The simplest model explaining SOL plasma flows is based on pressure gradients [46]. According to the magnetohydrodynamic momentum equation, particles will flow along magnetic field lines from regions of high pressure toward regions of minimum pressure ($v_{\parallel} \propto -\nabla_{\parallel} p$). In the SOL, where field lines are open, the divertor targets (downstream location) act as sinks for ions and the plasma pressure is therefore minimized, whereas the maximum pressure region (upstream location) is defined by the particle and heat coming from the core via radial transport. Ionization and heating within the SOL are for now neglected. In a first approximation, homogeneous radial transport leads to a pressure maximum at the geometrical center of each field line in between two targets (see figure 1). Once the particles have entered the SOL, the pressure gradient accelerates them and they stream along the field line towards the closest PFC, reaching the thermal ion sound speed c_s at the targets (Bohm–Chordura sheath criterion). A 'watershed' or 'stagnation point' with zero parallel flow velocity is formed at the maximum plasma pressure location along the field line. The counter-streaming flow pattern arises due to the fact that the straightened line in figure 1 winds around the plasma machine multiple times, leading to particle flows in opposite directions in closely adjacent spatial regions (figure 2(*c*)). Since the parallel flow is much faster than the perpendicular flow, the latter can be neglected in the analysis of the CIS measurements.

The above model shows that the structure of the flows is inherently linked to the magnetic field topology. In tokamaks, the single-null topology finds two counter-streaming flows that are spatially well separated by the X-point, whereas in stellarators the intrinsic 3D structure of the magnetic field should lead to a more complex flow structure.

In the particular case of W7-X, the magnetic islands connect different divertor modules while winding around the machine [47]. Different regions of an island have the shortest parallel connection to different divertor modules, and therefore two opposite flow directions are expected to be present within each island. This is illustrated in figures 2(*a*) and (*b*), where a single open field line is traced within one of the islands, and the two possible paths for the particles are

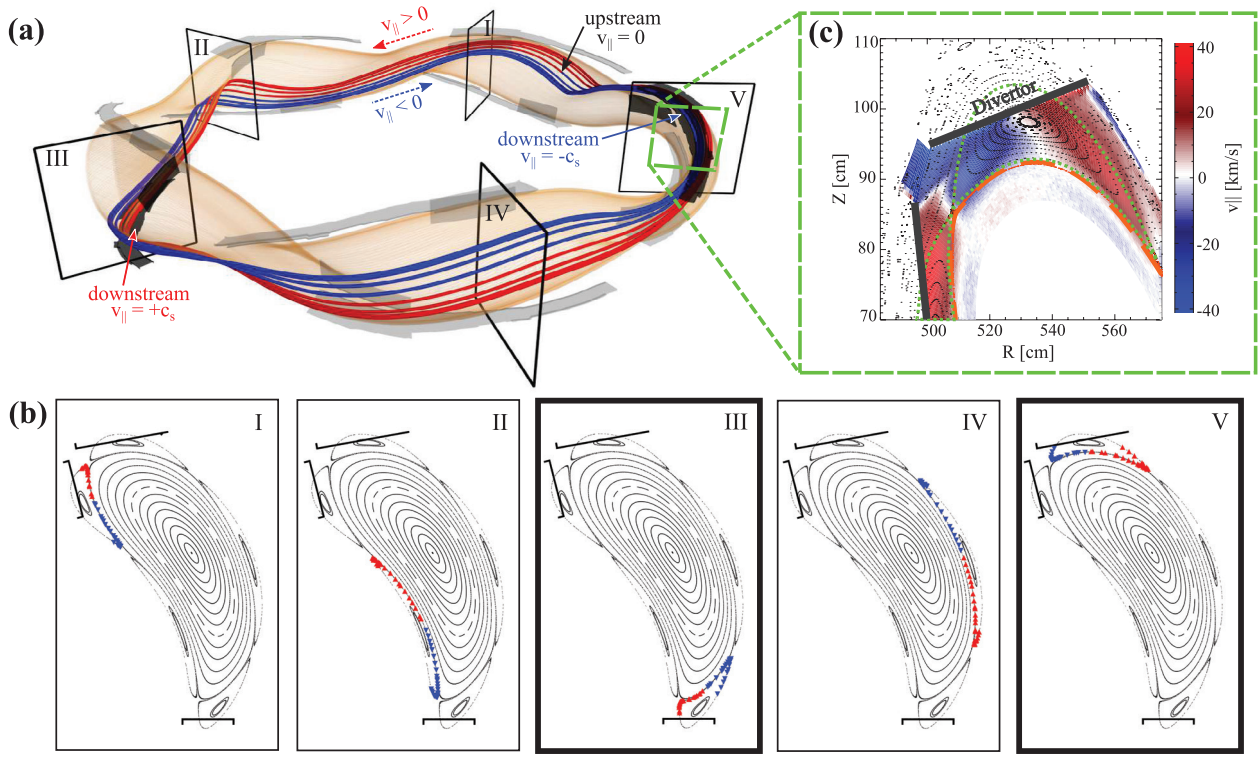

Figure 2. Plasma flow structure predicted for the W7-X island divertor, with focus on one magnetic island. The blue/red colour indicates domains along the field line being closer to a target in ± toroidal direction. (*a*) An open field line is traced from the upstream position to the closest targets (downstream location), highlighted in black (sections III and V in (*b*)). The upstream location (stagnation point) is the closest region to the confined core plasma and lies at the geometrical center of the field line. (*b*) Poloidal cross-sections at the locations I–V in (*a*), showing the field line counter-clockwise rotation in the machine. Note that the chosen field line interacts with the divertor targets only in sections III and V. (*c*) Poloidal cross-section of counter-streaming flows produced with EMC3-EIRENE. The flow structure is overlayed on a Poincaré plot showing the edge magnetic field, where the last closed flux surface is displayed in orange and the outermost surface of the islands is highlighted in green.

represented by blue and red. The composite flow pattern is a complex 3D structure of counter-streaming flows spatially close to each other, as shown in the poloidal cross-section in figure 2(*c*). A stagnation region is expected to be present at the center of, and in between, the magnetic islands.

A more complex physical model is used in EMC3-EIRENE, a fully 3D coupled plasma-fluid and kinetic edge transport Monte Carlo code [22, 48]. EMC3-EIRENE solves a set of Braginskii and kinetic transport equations for electrons, ions, neutral atoms and molecules in the plasma. One output is the parallel velocity of the main plasma species (hydrogen for W7-X in the last operational campaign) that is used to compare modelled and measured flows in the next section.

3. Experimental setup

The counter-streaming flow observation was carried out at W7-X, a stellarator characterized by the presence of ten island divertor modules interconnected by magnetic islands [43]. The coil system of W7-X allows flexibility in shaping the SOL, with varying rotational transform (ι), shear, and average toroidal curvature [47]. The presented measurements were performed in the *standard* and in the *low iota* magnetic configurations, characterized respectively by $\iota = 5/5$ and $\iota = 5/6$, which result in the formation of five and six magnetic islands in the machine edge [19, 49]. In the standard configuration, the five islands are five independent flux tubes, therefore their effect on the particle flows is relatively easy to distinguish. The low iota configuration features only one single flux tube that winds toroidally six times around the confined core plasma, showing up as six apparent islands in any poloidal cross section and therefore complicating the interpretation of the SOL geometry effects.

The flow measurements were performed using a CIS system [50], a diagnostic able to measure small wavelength variations (∼tens of pm) [51]. Its most recent applications are camera-based and exclusively sensitive to visible light, allowing for the observation of particle behavior in relatively cool plasma regions (up to hundreds of eV), e.g. in the edge region of fusion experiments. Examples of CIS implementations can be found for MAST [52], DIII-D [53–56], and ASDEX Upgrade [57]. We report observations from one of two systems installed on W7-X to measure impurity ion flow [58, 59], which views one divertor module tangentially (see figure 3(*a*)).

The CIS instrument at W7-X utilizes the *spatial heterodyne* detection technique, with birefringent crystals sandwiched between two polarizers, resulting in high optical throughput. An interference pattern is imposed across the entire plasma image, encoding information about the line-shift

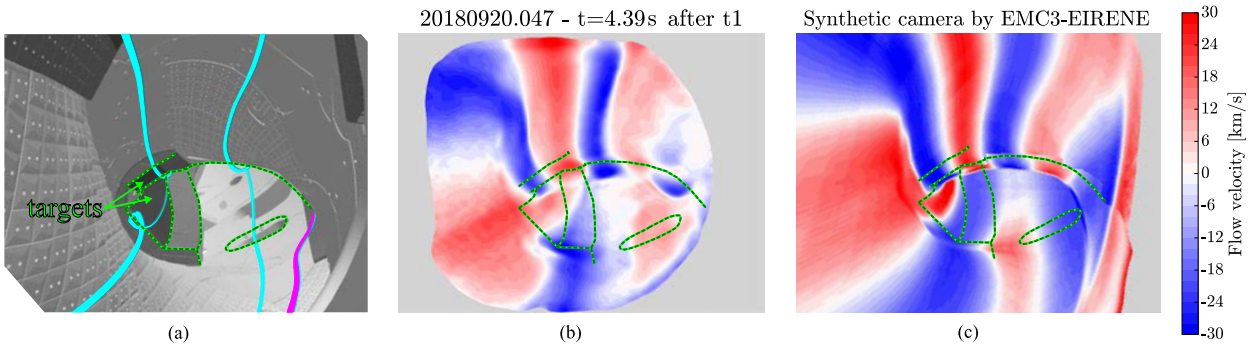

Figure 3. Comparison of C III flow velocity patterns. (*a*) In vessel geometry. The cyan and magenta lines indicate the position of the O-points of the five magnetic islands in the standard configuration. The magenta line indicates the island obscured by the experimental setup. (*b*) CIS measurement; (*c*) simulated flow from EMC3-EIRENE. The simulation was performed with an edge electron density of $n_e = 1 \times 10^{19}$ m^{-3}, input power of $P = 4$ MW (similar to measured quantities), and an anomalous cross-field diffusion coefficient of $D_\perp = \chi_{\perp,i,e} = 1.0$ m^2 s^{-1} (empirically determined). Blue/red indicate flows toward/away from the observation port. The *standard* W7-X magnetic configuration was used. The grey mask covers regions characterized by radiation brightness below 0.5% of the maximum.

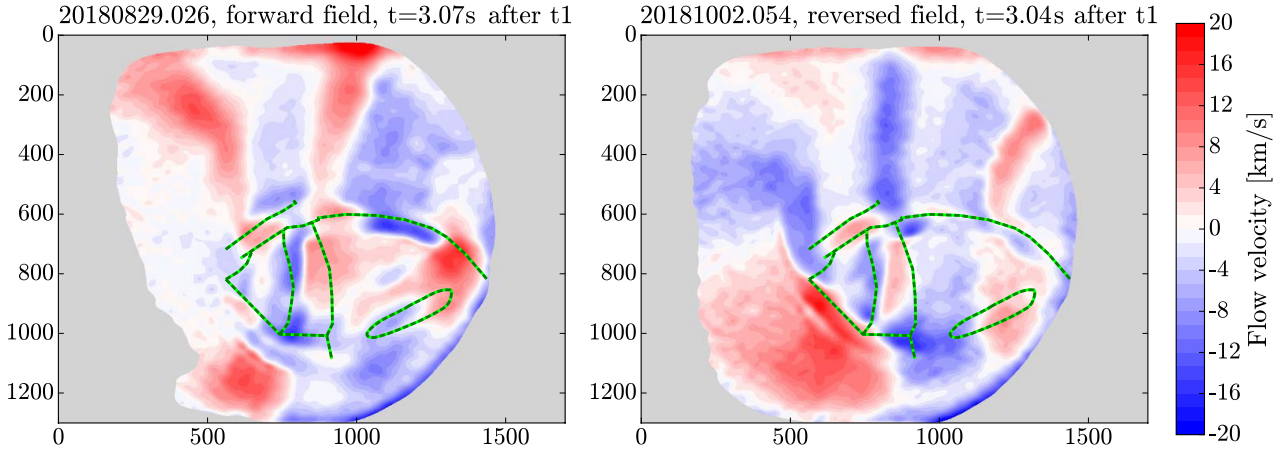

Figure 4. CIS measured C III flow velocities during magnetic field reversal experiments. Measurements performed in the *low-iota* magnetic configuration, with the line-integrated density and input power measured being $n_e = 6 \times 10^{19}$ m^{-2} and $P = 5$ MW respectively. (*a*) Forward and (*b*) reversed field configurations. Blue/red indicate flows toward/away from the observation port. The grey mask covers regions with radiation brightness below 0.5% of the maximum.

and broadening of a selected spectral line, i.e. the flow and temperature of one plasma species through the Doppler effect. These physical parameters can be recovered by a 2D (spatial) Fourier analysis of the images. For the diagnostic to function correctly, it is important to use a bandpass filter which is narrow enough to transmit spectral line emission from only one charged state of one species. More details about this technique can be found elsewhere [36, 51, 60].

The most important new feature of the W7-X CIS systems with relevance to the results presented, is the calibration source: a continuous tunable laser, allowing a precise and stable calibration of every spectral line in the range of interest (450–650 nm). The laser can also provide a direct measure of wavelength shifts in the same range as those expected from the plasma discharges (±30 pm), which is critical to accurately calibrate both the direction and the zero point of the impurity flow [61]. The use of calibration sources with even a few nm difference from the measured plasma emission has been shown to require complex corrections that cannot always be precisely determined [57, 62]. The measured spectral line presented here is the C III at 464.8811 nm, chosen because of its high intensity in the SOL region of W7-X. Carbon is intrinsically present in the W7-X SOL due to sputtering from graphite-based PFCs. The measurements present an uncertainty in the zero-point flow of ±6 km s^{-1}, which is significantly smaller than the reported flows and does not affect any of the conclusions.

4. Results

Counter-streaming structures are clearly visible in the measured flows, as shown in figure 3(*b*). One of the five independent islands of the standard configuration is obscured by in-vessel components, so that the pattern seen from the diagnostic port shows only eight flow channels, fitting with the prediction of two separate counter-streaming flows for each magnetic island. As expected from the simplified pressure driven model discussed above, the measured impurity flows are directed towards the nearest divertor modules.

For a comparison to theoretical predictions, 3D numerical simulations have been performed with the EMC3-EIRENE code, which is able to generate a synthetic CIS diagnostic for the above-mentioned experimental scenario [63]. The synthetic camera model provides line-integrated hydrogen ion flow velocities weighted by the C III emission intensity, which is calculated using ADAS photon-emission coefficients [64]. The impurity transport is computed based on a trace impurity fluid approach [65]. In high collisionality regime, the impurity flow is expected to be a good proxy for the main ion (hydrogen) flow due to frictional coupling [46]. The EMC3-EIRENE simulations for the presented scenarios support this assumption [23], making the CIS diagnostic applicable to study the bulk plasma flows of W7-X.

Figure 3(*c*) shows the C III flows from EMC3-EIRENE. Good qualitative agreement is found for most of the image, in particular in the four elongated flow structures in the top half, where the diagnostic lines of sight are shorter ($\leqslant$5 m) and intersect only one single island before hitting the wall. In the lower and right-hand sides, the interpretation is far more complex as the lines of sight are significantly longer ($\geqslant$6.5 m) and pass through multiple islands. In such cases, the reduced agreement is expected as the C III intensity distribution, on which the observed flow strongly depends, is more difficult to be precisely reproduced by EMC3-EIRENE. Additionally, the measured spectral integral is not necessarily a trivial function of the intensity weighted line averaged flow velocity, as is assumed by the simulation. Quantitatively, the direction and maximum of the flows measured in each island are similar to EMC3-EIRENE predictions.

Particles drifts, such as magnetic and $E \times B$ drifts, are not included in the current EMC3-EIRENE transport model. Nonetheless, it has been shown for tokamaks [66] and W7-AS [67–71] that these drifts are likely to play a role in the up-down asymmetries in the SOL, and could potentially affect the SOL flows by changing how the edge is populated. If ionization/recombination can be neglected, the only source defining the pressure profile (hence the flow pattern) is the outwards radial particle fluxes in the SOL, but this can change taking drifts into account. One possible experiment to assess the importance of drifts is the reversal of the magnetic field direction, as the particle drifts are expected to invert direction, whereas the anomalous cross-field transport is not [72, 73]. For the specific case of W7-X, the best magnetic configuration to highlight the contribution of drifts is the low iota configuration, as it is the least sensitive to error fields and it is characterized by the longest open field lines in the SOL ($\sim$1.5 times the length in the standard magnetic configuration on average) [74, 75].

Figure 4 shows CIS measurements in field reversal experiments for the low iota magnetic configuration. Apart from the field reversal, the two discharges are meant to be by design identical. In both forward and reversed field directions, the top portion of the images exhibits similar elongated structures that follow the magnetic island geometry, indicating the importance of the geometric considerations in the simplified pressure model above. The region around the divertor targets also shows a similar pattern. However, there are clear differences in the details of the structures. For example, the magnitude of the flow velocity is unbalanced, showing significantly higher values in $+/-v$ direction in case of forward/reversed field. Moreover, the elongated structures shows a partial rotation. Further analysis is necessary to determine the extent to which this can be attributed to drifts, but it is clear that CIS measurements do indeed show differences with field reversal. No such changes are seen in EMC3-EIRENE simulations that do not include drifts. Given the importance of understanding the SOL dynamics with respect to the heat exhaust problem, being able to investigate the potential role of drifts is crucial, and the CIS diagnostic seems to be able to provide a valuable contribution to this research area.

5. Conclusions

The CIS measurements presented here confirm the fundamental prediction of closely-spaced counter-streaming flows in the SOL of an island divertor. Stagnation regions are clearly present at the center of, and in between, the magnetic islands. Moreover, the measurements show C III flows streaming towards the nearest divertor modules, supporting the prediction that the target-sink action is dominant in our experiments, consistently with the EMC3-EIRENE modelling. CIS is therefore a powerful diagnostic for SOL plasma flow studies, in conjunction with the EMC3-EIRENE prediction of good collisional coupling of impurity and main ion flow in the plasma edge. This can lead to a better understanding of how the island divertor configuration affects the overall edge dynamics, that is particularly important with respect to the power exhaust problem. The W7-X CIS system also provides the first set of two-dimensional flow patterns comparing forward and reversed magnetic field experiments in an island divertor configuration. Although the results are yet to be fully understood, they demonstrate that field-reversal does impact the SOL parameters.

Acknowledgments

This work has been carried out within the framework of the EUROfusion Consortium and has received funding from the Euratom research and training program 2014–2018 and 2019–2020 under Grant agreement No. 633053. The views and opinions expressed herein do not necessarily reflect those of the European Commission. This work was supported in part by the U.S. Department of Energy (DoE) under Grants DE-SC0014529 and DE-SC0014210 along with start-up funds from the Physics Department at Auburn University, the Department of Engineering Physics and the College of Nuclear Engineering at the University of Wisconsin—Madison, USA. The publisher, by accepting the article for publication acknowledges, that the United States Government retains a non-exclusive, paid-up, irrevocable, world-wide license to publish or reproduce the published form of this manuscript, or allow others to do so, for United States Government purposes.

Special thanks to E. Scott and the Thomson scattering team for providing representative data used as input for the EMC3-EIRENE simulations, to S. Bozhenkov and H. Niemann for

the help with the field line tracer, and to M. Krause for the help with CATIA.

ORCID iDs

V. Perseo https://orcid.org/0000-0001-8473-9002
F. Effenberg https://orcid.org/0000-0002-4846-4598
D. Gradic https://orcid.org/0000-0002-6109-9345
T. Sunn Pedersen https://orcid.org/0000-0002-9720-1276

References

[1] ITER Physics Expert Group on Divertor, ITER Physics Expert Group on Divert Database, and ITER Physics Basis (ed) 1999 Chapter 4: Power and particle control *Nucl. Fusion* **39** 2391–469
[2] Linke J. 2006 High heat flux performance of plasma facing materials and components under service conditions in future fusion reactors *Fusion Sci. Technol.* **49** 455–64
[3] Wenniger R. *et al* 2015 DEMO exhaust challenges beyond ITER *42nd EPS Conf. on Plasma Physics (Lisbon, 22–26 June 2015)* (http://ocs.ciemat.es/EPS2015PAP/pdf/P4.110.pdf)
[4] Wenninger R. *et al* 2017 The DEMO wall load challenge *Nucl. Fusion* **57** 046002
[5] Philipps V. 2011 Tungsten as material for plasma-facing components in fusion devices *J. Nucl. Mater.* **415** S2–9
[6] Barabash V., Federici G., Matera R., Raffray A.R. and ITER Home Teams 1999 Armour materials for the ITER plasma facing components *Phys. Scr.* **T81** 74–83
[7] Behrisch R. and Prozesky V. 1990 Particle and power exhaust for a fusion plasma *Nucl. Fusion* **30** 2166
[8] Eich T., Sieglin B., Scarabosio A., Fundamenski W., Goldston R.J. and Herrmann A. 2011 Inter-ELM power decay length for JET and ASDEX Upgrade: measurement and comparison with heuristic drift-based model *Phys. Rev. Lett.* **107** 215001
[9] Loarte A. *et al* (The ITPA Scrape-off Layer and Divertor Group) 2007 Chapter 4: Power and particle control *Nucl. Fusion* **47** S203–63
[10] Pitcher C.S. and Stangeby P.C. 1997 Experimental divertor physics *Plasma Phys. Control. Fusion* **39** 779–930
[11] Reimold F., Wischmeier M., Bernert M., Potzel S., Kallenbach A., Müller H.W., Sieglin B. and Stroth U. 2015 Divertor studies in nitrogen induced completely detached H-modes in full tungsten ASDEX upgrade *Nucl. Fusion* **55** 033004
[12] Bernert M. *et al* (JET Contributors, The EUROfusion MST1 Team and The ASDEX Upgrade Team) 2017 Power exhaust by SOL and pedestal radiation at ASDEX Upgrade and JET *Nucl. Mater. Energy* **12** 111–8
[13] Bader A., Boozer A.H., Hegna C.C., Lazerson S.A. and Schmitt J.C. 2017 HSX as an example of a resilient non-resonant divertor *Phys. Plasmas* **24** 032506
[14] König R. *et al* 2002 The divertor program in stellarators *Plasma Phys. Control. Fusion* **44** 2365
[15] König R. *et al* 2004 Divertors for helical devices: concepts, plans, results, and problems *Fusion Sci. Technol.* **46** 152–66
[16] Morisaki T. *et al* 2005 Local island divertor experiments on LHD *J. Nucl. Mater.* **337–9** 154–60
[17] Feng Y. *et al* 2009 Comparative divertor-transport study for helical devices *Nucl. Fusion* **49** 095002
[18] Boozer A.H. and Punjabi A. 2018 Simulation of stellarator divertors *Phys. Plasmas* **25** 092505
[19] Renner H., Sharma D., Kißlinger J., Boscary J., Grote H. and Schneider R. 2004 Physical aspects and design of the Wendelstein 7-X divertor *Fusion Sci. Technol.* **46** 318–26
[20] Hirsch M. *et al* 2008 Major results from the stellarator Wendelstein 7-AS *Plasma Phys. Control. Fusion* **50** 053001
[21] Pedersen T.S. *et al* (The W7-X Team) 2018 First results from divertor operation in Wendelstein 7-X *Plasma Phys. Control. Fusion* **61** 014035
[22] Effenberg F. *et al* (The W7-X Team) 2019 Investigation of 3D effects on heat fluxes in performance optimized island divertor configurations at Wendelstein 7-X *J. Nucl. Mater. Energy* **18** 262–7
[23] Feng Y., Sardei F., Grigull P., McCormick K., Kisslinger J. and Reiter D. 2006 Physics of island divertors as highlighted by the example of W7-AS *Nucl. Fusion* **46** 807–19
[24] Feng Y., Frerichs H., Kobayashi M. and Reiter D. 2017 Monte-Carlo fluid approaches to detached plasmas in non-axisymmetric divertor configurations *Plama Phys. Control. Fusion* **59** 034006
[25] Goldston R.J. 2011 Heuristic drift-based model of the power scrape-off width in low-gas-puff H-mode tokamaks *Nucl. Fusion* **52** 013009
[26] LaBombard B. *et al* (The Alcator Group) 2004 Transport-driven scrape-off-layer flows and the boundary conditions imposed at the magnetic separatrix in a tokamak plasma *Nucl. Fusion* **44** 1047–66
[27] Garofalo A.M., Strait E.J., Johnson L.C., La Haye R.J., Lazarus E.A., Navratil G.A., Okabayashi M., Scoville J.T., Taylor T.S. and Turnbull A.D. 2002 Sustained stabilization of the resistive-wall mode by plasma rotation in the DIII-D tokamak *Phys. Rev. Lett.* **89** 235001
[28] Kobayashi M., Morita S. and Goto M. 2017 Space-resolved visible spectroscopy for two-dimensional measurement of hydrogen and impurity emission spectra and of plasma flow in the edge stochastic layer of LHD *Rev. Sci. Instrum.* **88** 033501
[29] Kobayashi M., Morita S. and Goto M. 2017 2D distribution of hydrogen/impurity radiation and flow formation in stochastic layer during detachment transition in LHD *Nucl. Mater. Energy* **12** 1043–8
[30] Kobayashi M. *et al* 2007 Divertor transport study in the Large Helical Device *J. Nucl. Mater.* **363–5** 294–300
[31] Feng Y. *et al* 2008 Fluid features of the stochastic layer transport in LHD *Nucl. Fusion* **48** 024012
[32] Feng Y. 2003 Modelling of island divertor physics and comparison to W7-AS experimental results *J. Nucl. Mater.* **313–6** 857–62
[33] Feng Y., Kobayashi M., Lunt T. and Reiter D. 2011 Comparison between stellarator and tokamak divertor transport *Plasma Phys. Control. Fusion* **53** 024009
[34] Effenberg F. *et al* (The W7-X Team) 2017 Numerical investigation of plasma edge transport and limiter heat fluxes in Wendelstein 7-X startup plasmas with EMC3-EIRENE *Nucl. Fusion* **57** 036021
[35] Ezumi N., Kobayashi T., Ohno N., Sawada K., Takamura S., Kobayashi M., Masuzaki S. and Feng Y. 2009 Experimental observation of plasma flow alternation in the LHD stochastic magnetic boundary *J. Plasma Fusion Res. Ser.* **8** 429–32
[36] Howard J., Michael C., Glass F. and Danielsson A. 2003 Time-resolved two-dimensional plasma spectroscopy using coherence-imaging techniques *Plasma Phys. Control. Fusion* **45** 1143–66
[37] Feng Y., Sardei F., Grigull P., McCormick K., Kisslinger J., Reiter D. and Igitkhanov Y. 2002 Transport in island divertors: physics, 3D modelling and comparison to first experiments on W7-AS∗ *Plasma Phys. Control. Fusion* **44** 611

[38] Reiter D., Baelmans M. and Börner P. 2005 The EIRENE and B2-EIRENE codes *Fusion Sci. Technol.* **47** 172–86

[39] Kobayashi M. *et al* 2013 Edge impurity transport study in the stochastic layer of LHD and the scrape-off layer of HL-2A *Nucl. Fusion* **53** 033011

[40] Morita S. 2013 Effective screening of iron impurities in the ergodic layer of the Large Helical Device with a metallic first wall *Nucl. Fusion* **53** 093017

[41] Morita S. *et al* 2014 Two-dimensional study of edge impurity transport in the Large Helical Device *Plasma Phys. Control. Fusion* **56** 094007

[42] Akerson A.R., Bader A., Hegna C.C., Schmitz O., Stephey L.A., Anderson D.T., Anderson F.S.B. and Likin K.M. 2016 Three-dimensional scrape off layer transport in the helically symmetric experiment HSX *Plasma Phys. Control. Fusion* **58** 084002

[43] Feng Y., Beidler C.D., Geiger J., Helander P., Hölbe H., Maassberg H., Turkin Y. and Reiter D. 2016 On the W7-X divertor performance under detached conditions *Nucl. Fusion* **56** 126011

[44] Zhang H. *et al* 2017 Vertical profiles and two-dimensional distributions of carbon line emissions from C2+-C^{5+} ions in attached and RMP-assisted detached plasmas of large helical device *Phys. Plasmas* **24** 022510

[45] Oishi T., Morita S., Dai S.Y., Kobayashi M., Kawamura G., Huang X.L., Zhang H.M., Liu Y. and Goto M. 2017 Observation of carbon impurity flow in the edge stochastic magnetic field layer of Large Helical Device and its impact on the edge impurity control *Nucl. Fusion* **58** 016040

[46] Stangeby P.C. 2000 *The Plasma Boundary of Magnetic Fusion Devices* (Bristol: IOP Publishing)

[47] Hölbe H. 2015 Control of the magnetic topology and plasma exhaust in the edge region of Wendelstein 7-X: a numerical study *PhD Thesis* Max Planck Institute for Plasma Physics (https://pure.mpg.de/rest/items/item_2250904/component/file_2250907/content)

[48] Feng Y., Sardei F. and Kisslinger J. 1999 3D fluid modeling of the edge plasma by means of a Monte Carlo technique *J. Nucl. Mater.* **266–9** 812–8

[49] Andreeva T. 2002 Vacuum magnetic field configurations of Wendelstein 7-X *Technical Report* IPPIII/270, Max Planck Institute for Plasma Physics (https://pure.mpg.de/rest/items/item_2138236_1/component/file_2138235/content)

[50] Howard J. 1990 Novel scanning interferometer for two-dimensional plasma density measurements *Rev. Sci. Instrum.* **61** 1086–94

[51] Howard J. 2010 Coherence imaging spectro-polarimetry for magnetic fusion diagnostics *J. Phys. B: At. Mol. Opt. Phys.* **43** 144010

[52] Silburn S.A., Harrison J.R., Howard J., Gibson K.J., Meyer H., Michael C.A. and Sharples R.M. 2014 Coherence imaging of scrape-off-layer and divertor impurity flows in the mega amp spherical tokamak (invited) *Rev. Sci. Instrum.* **85** 11D703

[53] Howard J. *et al* 2011 Coherence imaging of flows in the DIII-D divertor *Contrib. Plasma Phys.* **51** 194–200

[54] Samuell C.M., Porter G.D., Meyer W.H., Rognlien T.D., Allen S.L., Briesemeister A., Mclean A.G., Zeng L., Jaervinen A.E. and Howard J. 2018 2D imaging of helium ion velocity in the DIII-D divertor *Phys. Plasmas* **25** 056110

[55] Samuell C.M., Allen S.L., Meyer W.H., Isler R.C., Briesemeister A., Wilcox R.S., Lasnier C.J., Mclean A.G. and Howard J. 2018 Verification of Doppler coherence imaging for 2D ion velocity measurements on DIII-D *Rev. Sci. Instrum.* **89** 093502

[56] Allen S.L., Samuell C.M., Meyer W.H. and Howard J. 2018 Laser calibration of the DIII-D coherence imaging system *Rev. Sci. Instrum.* **89** 10E110

[57] Gradic D., Ford O.P., Burckhart A., Effenberg F., Frerichs H., König R., Lunt T., Perseo V. and Wolf R.C. 2018 Doppler coherence imaging of divertor and SOL flows in ASDEX upgrade and Wendelstein 7-X *Plasma Phys. Control. Fusion* **60** 084007

[58] Perseo V., König R., Biedermann C., Ford O., Gradic D., Krychowiak M., Kocsis G., Ennis D., Maurer D. and Pedersen T.S. 2017 Coherence imaging spectroscopy systems on Wendelstein 7-X for studies of island divertor plasma behavior *44th EPS Conf. on Plasma Physics (Belfast, 26–30 June 2015)* (http://ocs.ciemat.es/EPS2017PAP/pdf/P5.103.pdf)

[59] Perseo V., Gradic D., König R., Ford O.P., Killer C., Grulke O., Ennis D.A. and The W7-X Team 2019 Validation of coherence imaging spectroscopy at Wendelsteain 7-X for impurity flow measurements *Rev. Sci. Instrum.* (submitted)

[60] Howard J. *et al* 2010 Doppler coherence imaging and tomography of flows in tokamak plasmas (invited) *Rev. Sci. Instrum.* **81** 10E528

[61] Gradic D., Perseo V., König R. and Ennis D. 2019 A new calibration implementation for Doppler coherence imaging spectroscopy *Fusion Eng. Des.* **146A** 995–8

[62] Samuell C.M., Allen S.L., Meyer W.H. and Howard J. 2017 Absolute calibration of Doppler coherence imaging velocity images *J. Instrum.* **12** C08016

[63] Frerichs H. *et al* 2016 Synthetic plasma edge diagnostics for EMC3-EIRENE, highlighted for Wendelstein 7-X *Rev. Sci. Instrum.* **87** 11D441

[64] Summers H.P. 1994 *Atomic data and Analysis Structure: User Manual* (Abingdon: Joint European Torus)

[65] Feng Y. *et al* 2001 Numerical studies on impurity transport in the W7-AS island divertor *28th EPS Conf. on Controlled Fusion and Plasma Physics. Contributed Paper* (*ECA* vol 25A) ed C. Silva *et al* (Funchal: European Physical Society) pp 1949–52

[66] Petrie T.W. *et al* 2001 The effect of divertor magnetic balance on H-mode performance in DIII-D *J. Nucl. Mater.* **290–3** 935–9

[67] Feng Y., Herre G., Grigull P. and Sardei F. 1998 The effects of field reversal on the W7-AS island divertor at low densities *Plasma Phys. Control. Fusion* **40** 371

[68] Feng Y., Sardei F., Grigull P. and Herre G. 1999 Drift effects in W7-AS limiter and island divertor configurations *J. Nucl. Mater.* **266–9** 928–33

[69] Grigull P. *et al* 2003 Influence of magnetic field configurations on divertor plasma parameters in the W7-AS stellarator *J. Nucl. Mater.* **313–6** 1287–91

[70] Grigull P. *et al* 2003 Divertor operation in stellarators: results from W7-AS and implications for future devices *Fusion Eng. Des.* **66–8** 49–58

[71] McCormick K., Grigull P., Burhenn R., Ehmler H., Feng Y., Giannone L., Haas G. and Sardei F. 2005 Neutral pressure behavior for diverted discharges in the Wendelstein 7-AS stellarator *J. Nucl. Mater.* **337–9** 520–4

[72] Chankin A.V. 1997 Classical drifts in the tokamak sol and divertor: models and experiment *J. Nucl. Mater.* **241–3** 199–213

[73] Birkenmeier G., Ramisch M., Manz P., Nold B. and Stroth U. 2011 Experimental investigation of the magnetic configuration dependence of turbulent transport *Phys. Rev. Lett.* **107** 025001

[74] Hammond K.C. *et al* (The W7-X Team) 2019 Drift effects on W7-X divertor heat and particle fluxes *Plasma Phys. Control. Fusion* (submitted)

[75] Sinha P., Hölbe H., Pedersen T.S. and Bozhenkov S. 2017 Numerical studies of scrape-off layer connection length in Wendelstein 7-X *Nucl. Fusion* **58** 016027